Available online at www.sciencedirect.com

jmr&t Journal of Materials Research and Technology

journal homepage: www.elsevier.com/locate/jmrt

Original Article

Influence of 17-4 PH stainless steel powder recycling on properties of SLM additive manufactured parts

Sara Giganto [a], *Susana Martínez-Pellitero* [a,*], *Joaquín Barreiro* [a], *Pablo Zapico* [b]

[a] *Area of Manufacturing Engineering, Universidad de León, 24071, León, Spain*
[b] *Department of Construction and Manufacturing Engineering, University of Oviedo, Oviedo, Spain*

ARTICLE INFO

Article history:
Received 18 October 2021
Accepted 18 December 2021
Available online 23 December 2021

Keywords:
17-4 PH stainless steel
Additive manufacturing (AM)
Mechanical properties
Metallic powder reuse
Powder bed fusion (PBF)
Selective laser melting (SLM)

ABSTRACT

Metal Additive Manufacturing (AM) processes are developing quickly. These processes have several attractive qualities, however, the quality of manufactured parts still remains a major issue that needs to be addressed if it is to become a prevalent technology in the industry. In some powder bed fusion techniques, such as Selective Laser Melting (SLM), there is a portion of initial powder that does not melt and it can be recycled to ensure the economic and environmental viability of the process. In previous research, we demonstrated the morphological, chemical and microstructural change suffered by 17-4 PH stainless steel powder after reusing it in a SLM manufacturing process. In this work, the properties of 17-4 PH stainless steel parts, printed from powder in different recycling states (virgin powder (P_0) and 20 times reused powder (P_{20})), were evaluated, in order to establish good recycling procedures and optimise the SLM process performance. Analyses of the properties revealed a slight decrease in roughness and pore size with powder recycling. The external porosity of the samples is similar in both powder states; however, internal porosity decreases by increasing the number of reuse cycles. Regarding the microstructural analysis, a slight increase in the γ-phase is observed with the powder recycling, which leads to a slight increase in ductility and decrease in hardness of the samples. Therefore, it is concluded that the 17-4 PH powder recycling process in SLM manufacturing is adequate and recommended to ensure the economic and environmental viability of the process without adversely affecting the properties of the parts.

1. Introduction

Powder Bed Fusion (PBF) processes produce parts by Additive Manufacturing (AM) (layer by layer) using powder as raw material. For metal part manufacturing, this technique includes the processes of Direct Metal Laser Deposition (DMLS), Selective Laser Sintering (SLS), Selective Laser Melting (SLM) and Electron Beam Melting (EBM). In these processes, the layer of metal powder deposited on the build-plate is sintered (DMLS and SLS) or melted (SLM and EBM), using a

* Corresponding author.
E-mail address: smarp@unileon.es (S. Martínez-Pellitero).
https://doi.org/10.1016/j.jmrt.2021.12.089

laser (DMLS, SLS and SLM) or an electron beam (EBM) as a heat energy source. After finishing a PBF manufacturing process, the leftover powder (unmelted powder) is aspirated and sieved for reuse in order to ensure the economic and environmental viability of the process.

Reusing powder is a viable strategy to improve the AM economy. The use of powder from previous builds results in direct cost savings, making AM more competitive and enabling wider use of AM to allow design flexibility and custom product offerings [1]. Studies have also shown an improvement in repeatability of printed parts as the number of powder recycles increases [2].

As metal AM is adopted more widely in the aerospace, automotive and medical industries, there is a growing demand to improve part quality and reduce overall cost. A critical factor for creating variations in the properties of PBF parts is the raw material, where changes in powder properties, due to reuse, can potentially affect process performance. Several researchers have focused on the analysis of reused powder in PBF manufacturing.

The influence of metallic powder reuse on its oxidation is one of the aspects studied. Montelione et al. [3] demonstrated the importance of managing/mitigating raw material oxidation in Ti–6Al–4V metallic powder to improve its reuse and increase its useful life in EBM manufacturing. Sutton et al. [4] related the increase in oxygen content of 304L stainless steel powder, after its reuse in the SLM manufacturing process, to a decrease in impact hardness. However, in their study, the tensile properties did not change with reuse, revealing the differences between the static and dynamic properties. Despite the progressive deformation of the particles and the increase in oxidation, Ghods et al. [5] concluded that there was no discernible change in the porosity of the Ti–6Al–4V metallic powder after its reuse in the EBM process. Similarly, regarding fatigue behaviour, the study carried out by Schiltz et al. [1] did not detect significant changes with the metal powder reuse of Ti–6AlV–4VAl and 316L and 17-4 PH stainless steels in DMLS manufacturing. On the other hand, an improvement in certain mechanical properties of PBF-manufactured parts has also been obtained with an increase in the oxidation of reused powder. For example, Tang et al. [6] obtained an increase in both the Yield Tensile Strength (YTS) and the Ultimate Tensile Strength (UTS) of Ti–6Al–4V EBM parts by increasing powder reuse cycles from 6 to 21.

Another factor that affects the properties of PBF parts is the presence of spatter particles [7]. These particles are formed during the material melting process. According to the research of Wang et al. [8], the presence of spatter particles in reused Co–Cr–W powder favours pore formation and severely affects the mechanical properties of SLM parts. This aspect significantly reduces tensile strength, yield strength and elongation values after six powder reuse cycles. Likewise, Ahmed et al. [9] observed that spatter/agglomerate particles are, potentially, the cause of decreasing quality in 17-4 PH SLM printed parts. In this study the authors identified an increase in pore size and surface roughness, as well as a decrease in failure strain with powder reuse. However, the powder reuse did not affect the tensile properties or microstructure of the printed parts.

Other researchers, such as Gorji et al. [10] or Terrassa et al. [11], concluded that there were no significant changes in the mechanical properties of 316L stainless steel printed parts based on a certain number of powder reuse cycles. Despite the substantial changes in powder properties found with reuse (density decreases slightly, ductility increases slightly, and UTS and YTS remain relatively consistent), it appears that 316L stainless steel powder can be used for multiple builds with limited changes in the mechanical properties of the SLM parts [12]. Likewise, Yi et al. [13] concluded that reuse of Inconel 718 powder between 1 and 14 times has no negative effect on the mechanical properties of SLM parts. In the case of DMLS parts of Ti–6Al–4V, Alamos et al. [14] proved that titanium powder can be recycled up to 8 times without compromising the part properties (YTS, UTS, elongation, reduction in area and density).

After analysing the effect of metallic powder reuse and, in order to minimise the risk of defect formation and to extend the powder reuse to a greater number of PBF cycles, several researchers have proposed recycling methodologies. Pinto et al. [15] recommended a magnetic separation process after sieving, or providing a quantitative assessment of the virgin/reused powder ratio to ensure homogeneity of the powder bed, in terms of particle packing and layer distribution during 316L stainless steel SLM processing. Ardila et al. [16] proposed an IN718 powder recycling methodology that allows its reuse in up to 14 cycles, while maintaining the properties of SLM parts, both metallurgically (in terms of equivalent microstructure and porosity) and mechanically (in terms of similar hardness). Based on the results obtained in their research, Cordova et al. [17] concluded that it is feasible to reuse Al–Mg-Sc-Zr powder in four subsequent SLM manufacturing cycles after proper powder sieving and a rejuvenation step, mixing 40% of virgin powder. Both the powder and the part exhibited similar properties when comparing the virgin powder and the powder reused four times. On the other hand, Powell et al. [18] proposed plasma spheroidisation as a promising method to avoid powder disposal at the end of their useful life, creating particles similar to virgin powder. This is an economically viable proposal to reduce waste.

The process of metallic powder reuse in PBF manufacturing is an important factor to ensure the quality of final parts. In spite of this, SLM parts manufactured with 17-4 PH stainless steel powder have only been evaluated in processing conditions with an inert argon atmosphere and high laser power (about 200 W) [1,8]. However, the effect of recycling 17-4 PH powder on the quality of parts processed by SLM in an inert nitrogen atmosphere using low laser power (as is the case of parts manufactured using the ProX100 3DSystems machine for dental applications and others) has not yet been studied. Our study focuses in this issue.

In previous research, we carried out the characterisation of 17-4 PH metallic powder at different states (virgin powder and 10 and 20 times recycled powder). The results showed morphological, chemical and microstructural changes in the powder [19]. In the current study, the characterisation of SLM 17-4 PH stainless steel manufactured parts is afforded (porosity, roughness, tensile strength, microstructure, hardness and microhardness) using virgin powder and 20 times

recycled powder. This study allows the evaluation of the quality of SLM parts obtained from powder under different reuse conditions, as well as the proper reuse process.

2. Materials and methods

2.1. SLM manufacturing

A Direct Metal Printing ProX 100 SLM machine (distributed by 3DSystems) [20] was used to manufacture the test parts. Inert nitrogen gas was used during the manufacturing process. According to previous research [21], the main SLM parameters were setup at: 38 W of laser power (P), 140 mm/s of scanning speed (v), 70 μm of hatch distance (h) and a layer thickness (l_t) of 30 μm. The combination of these parameters (according to Eq. (1)) provides the value of the Volumetric Energy Density (VED) or the amount of energy delivered per unit volume of powder bed, i.e. 129 J/mm^3. The hexagonal scanning strategy was used, in order to reduce surface stress generated during the powder bed melting process. Likewise, this laser scanning strategy is recommended by the manufacturer and other researchers to achieve high density [22] and good mechanical properties [23] in SLM parts.

$$VED\ [J/mm^3] = \frac{P\ [W]}{v[mm/s]\cdot h[mm]\cdot l_t[mm]} \quad (1)$$

After SLM manufacturing, the leftover powder was vacuumed and sieved for reusing. A 3DSystems PX-BOX connected to the SLM machine was used to sieve the metallic powder by means of a 75 μm mesh sieve.

According to manufacturer recommendations and other researchers [24], a stress relieving, post-process Heat Treatment (HT) was applied to the 17-4 PH stainless steel part/build-plate sets after SLM printing. This treatment consisted of heating the component and keeping it at 650° for 2 h, followed by air cooling. Finally, the test parts were split from the build-plate by means of Wire Electrical Discharge Machining (WEDM).

The variation of both the SLM parameters and the post-process HT gave rise to variation in part properties [25]. In this study, SLM manufacturing and post-process HT conditions were identical for all the evaluated samples, the only variable being the starting powder (2.2 section). In this way, the results reveal the real influence of powder recycling.

2.2. Metallic powder

In this study, 17-4 PH stainless steel powder (supplied by 3DSystems [26]) was used for manufacturing the parts. The chemical composition is shown in Table 1. This alloy combines high tensile strength, fracture toughness and corrosion resistance. The excellent mechanical properties are of great interest to the aerospace, automotive and metal injection moulding industry, as well as marine environments or power plants [27]. Among other stainless steels, 17-4 PH is one of the most common metallic materials for medical tools and devices, due to a combination of good wear resistance, high strength, affordability, biocompatibility and manufacturability [28].

In our study, test parts were manufactured using two conditions:

- **P_0**: virgin powder, as received from the supplier (Fig. 1a).
- **P_{20}**: 20 times recycled powder (Fig. 1b).

The Particle Size Distribution (PSD) of both powder states is shown in Fig. 2. As analysed in previous work [19], the virgin powder (P_0) presented the smallest particle size, which increased when reusing the powder.

Figure 3 shows the results of the XRD analysis of the P_0 and P_{20} powder [19]. As shown in Fig. 3, the phase proportions vary slightly when reusing the stainless steel powder, with a slight increase of the γ-phase.

2.3. Test samples

A sample set was designed to characterise the properties of 17-4 PH stainless steel parts, taking advantage of the printing

Table 1 – Chemical composition of 17-4 PH stainless steel powder [26].

Element	Fe	Cr	Ni	Cu	Si	Mn	Nb
% of weight	Balance	15–17.5	3–5	3–5	<1	<1	0.15–0.45

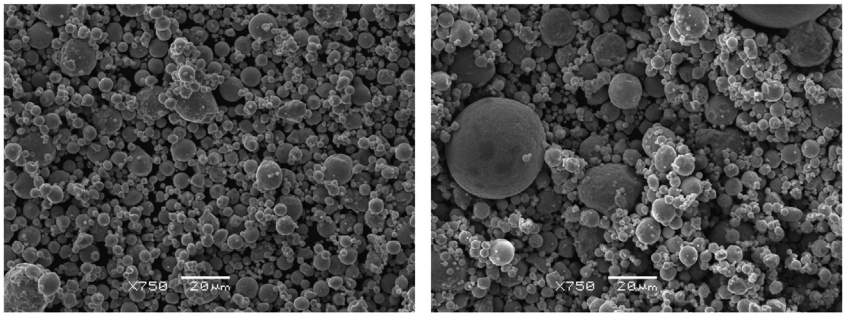

Fig. 1 – SEM images at 750x magnification: (a) P_0 and (b) P_{20}.

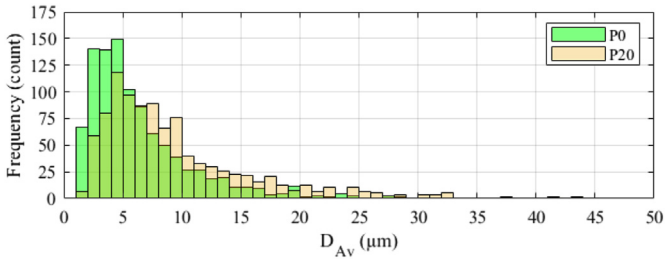

Fig. 2 – PSD related to the average diameters detected for each powder state: P_0 and P_{20}.

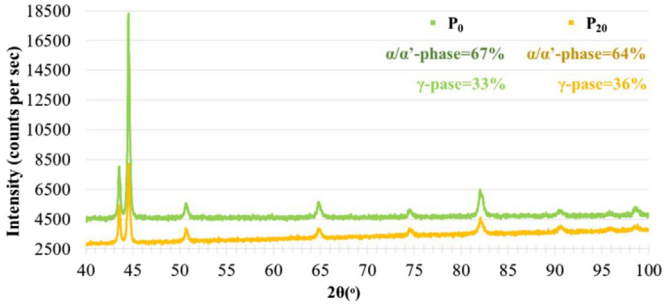

Fig. 3 – Schematic XRD results obtained for P_0 and P_{20} powder.

surface available on the SLM manufacturing build-plate. The sample set (Fig. 4) consisted of:

- A 25 mm size cube to analyse density/porosity and roughness.
- Three tensile samples to evaluate tensile strength.
- Three 10 mm size cubes to study internal porosity, microstructure, hardness and microhardness.

One of the 10 mm cubes was used for analysing the microstructure by X-Ray Diffraction (XRD). The other two were cut in half (Fig. 4) using a metallographic cutting machine: one in a perpendicular direction to the manufactured layers or a longitudinal direction, resulting in the two samples L_1 and L_2; the other was cut in a parallel direction to the manufactured layers or transverse direction, resulting in the two samples T_1 and T_2. These samples were used for analysing internal porosity, microstructure by chemical attack, hardness and microhardness. In this way, in addition to analysing these properties, their variation as a function of direction (transversal and longitudinal) was also studied. The cut samples were encapsulated in resin and polished for further analysis.

2.4. *Analysed properties*

2.4.1. *Density/porosity*

Part density was calculated by the Archimedes principle using demineralised water, a reliable method for estimating the porosity rate of SLM parts [29]. A CB-Complet precision electronic balance, with a precision of 0.001 g, was used for sample mass measurements. The sample part used for Archimedes testing was the 25 mm size cube.

In addition, an Olympus BHM-312 L Optical Microscope (OM) at 50x magnification was used for analysing the internal porosity. Mosaics of images that make up the polished internal surfaces of the cut samples (L_1, L_2, T_1 and T_2) were created and analysed using ImageJ software.

2.4.2. *Roughness*

A SJ-500 Mitutoyo surface roughness measuring system was used for roughness measurements. The test was carried out with a probe tip of 5 μm radius, 2.5 mm sampling length and 12.5 mm evaluation length, according to ISO 4288 (1996) [30]. The profile parameters analysed for roughness assessment were the arithmetical mean roughness (R_a) and the total height of roughness profile (R_t). Results were obtained using 10 measurements at each face of the 25 mm cube.

2.4.3. *Microstructure*

The polished surface of T_1, T_2, L_1 and L_2 samples was etched with Vilella to reveal the phases. Microstructure images were taken with the OM at 100x magnification.

An XRD test of the samples was carried out using a Bruker D8 Discover machine equipped with a Cu anode ($\lambda = 1.5418$ Å). These tests were performed on both the lateral and top faces of the samples using a two-theta range of 40–100° at room temperature. This analysis allows the searching and matching of phases present in polycrystalline samples (such as those analysed in this study), as well as to determine the relative proportions using the procedure described in the ASTM E975-13 standard [31] to determine the retained austenite proportion in steel with a near random crystallographic orientation.

2.4.4. *Hardness and microhardness tests*

The polished surface of the samples, cut transversely (T_1 and T_2) and longitudinally (L_1 and L_2), was subjected to hardness and microhardness tests using a Shimadzu HMW-2000 tester and according to ISO 6507–1 (2018) [26]. Microhardness tests

were performed on the etched surfaces of the samples in the different phases following the Vickers HV0.01 procedure. The microhardness results were obtained using 5 measurements taken on each phase of four sections (T_1, T_2, L_1 and L_2) of each sample (P_0 and P_{20}). Hardness tests were carried out at 9 points of the surface (distributed in a matrix of 2.5 mm equidistant points) following the Vickers HV2 procedure.

2.4.5. *Tensile test*

The tensile sample was designed according to the recommendations in ISO 6892–1 (2019) standard [32]. The tensile testing was carried out using a Servosis ME-402/5 universal testing machine, with the parameter configuration according to ISO 6892–1 (2019) standard [32] for rectangular cross-section samples.

3. Results and discussion

3.1. *Density/porosity*

Figure 5 shows the porosity analysis of P_0 and P_{20} samples. The total porosity percentage is 1.18% and 1.02% for P_0 and P_{20}, respectively. This means a 0.16% decrease in porosity with powder reuse. The external porosity (P_e) is almost the same for both conditions. More variability is found in the internal porosity (P_i) between the parts manufactured using virgin powder and those using reused powder.

The study of internal porosity, using images obtained with the OM and analysed with the ImageJ software (Fig. 6), provide more detailed information about the samples' pores. Regarding the average pore size, a value of 82 μm^2 was obtained for the P_0 samples and 50 μm^2 for the P_{20} samples, which shows that, in general, the pore size is larger in the P_0 samples. Likewise, the highest maximum pore area value was obtained in the P_0 samples, reaching a value of 6535 μm^2 compared to the 4542 μm^2 obtained in the P_{20} samples. The minimum pore size in both types of powder was 0.5 μm^2.

The pores circularity (Eq. (2)) is slightly higher in the parts manufactured with reused powder, obtaining average values of 0.78 and 0.81 for P_0 and P_{20}, respectively.

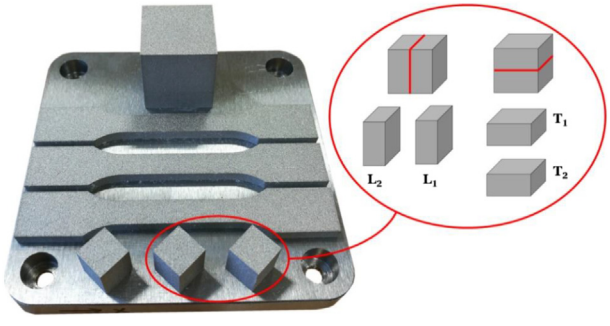

Fig. 4 – Test samples manufactured using SLM with 17-4 PH stainless steel.

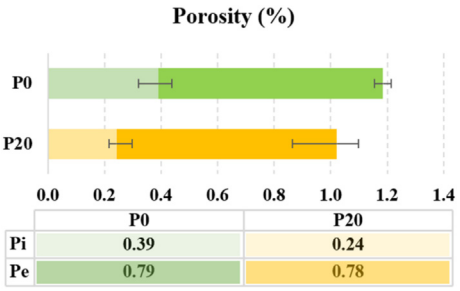

Fig. 5 – Porosity results of P_0 and P_{20} samples.

$$Circularity = \frac{4\pi \cdot Area}{Perimeter^2} \quad (2)$$

Analysing the number and circularity of the pores as a function of their size in more detail, a clear trend is observed, decreasing with the increase in size (Fig. 7 and Fig. 8). The circularity values as a function of pore size conform to a logarithmic function, that is, it decreases rapidly and then levels out (Fig. 7). The graph of the number of pores as a function of their size fits a potential function perfectly (Fig. 8). Both trends are observed in both samples manufactured with P_0 and P_{20} powder, without any major difference between them.

Spherical pores are usually the result of gases trapped in the melting pool due to an excessive energy input and high cooling rates during the solidification process. Such porosity is randomly distributed in SLM parts and it is difficult to remove completely. Lack-Of-Fusion (LOF) defects are mainly due to the lack of energy input during the SLM process and are usually distributed between the scan tracks and the deposited layers [33].

From the results obtained in this section, it can be concluded that the porosity decreases slightly with powder reuse. Also, the SLM process using reused powder results in parts that have pores which are generally smaller in size and greater in circularity. Regarding internal porosity, the results are similar in both the perpendicular (longitudinal section) and parallel (transversal section) directions to the manufactured layers.

3.2. *Roughness*

Roughness of the manufactured parts decreases with powder reuse (Fig. 9). The arithmetical mean roughness of the evaluated profile (R_a) decreases 2.25 μm after 20 powder reuses, while the total height of the roughness profile (R_t) is reduced by 11.76 μm.

Figure 9 shows the average values of the studied parts. Additional conclusions are extracted when the results from the top and lateral cube's external faces are analysed in more detail (Table 2). As expected, the highest roughness values were obtained on the top surface of the samples for both types of powder. In this face the marks of the laser scanning strategy become visible, characterised by hexagonal patches.

For a final application, mechanical post-processes such as sandblasting are usually applied to SLM parts in order to

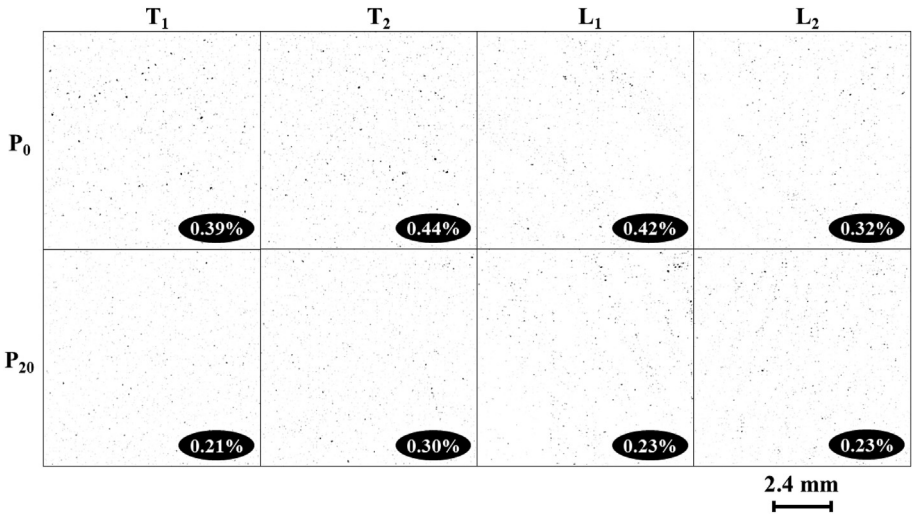

Fig. 6 – Analysis of internal porosity using ImageJ software on T_1, T_2, L_1 and L_2 surfaces of P_0 and P_{20} samples.

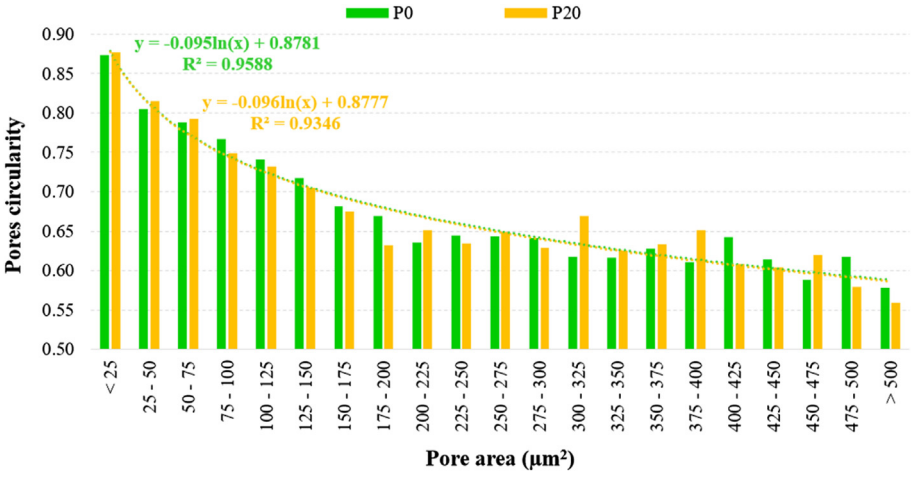

Fig. 7 – Pore circularity as a function of pore size for P_0 and P_{20} samples.

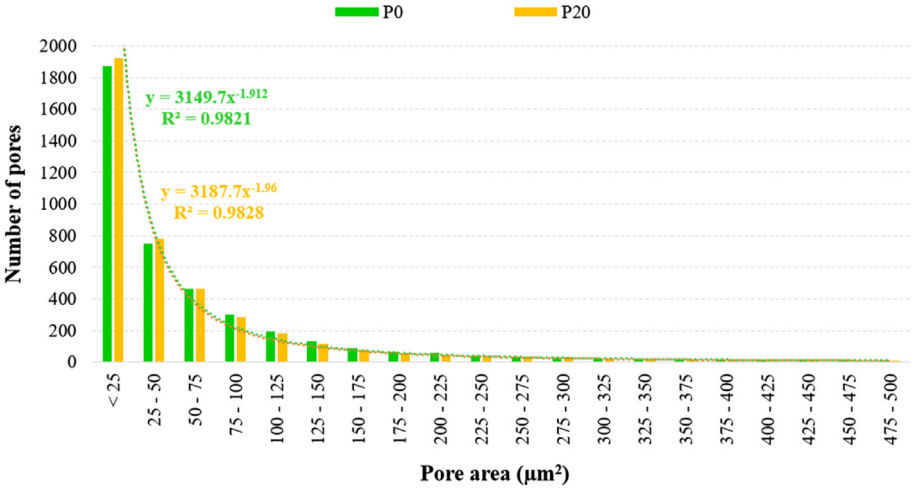

Fig. 8 – Number of pores as a function of pore size for P_0 and P_{20} samples.

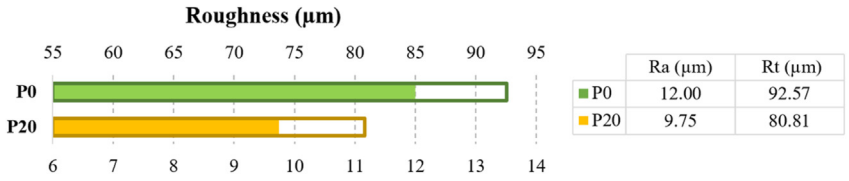

Fig. 9 – Roughness results (R_a and R_t) for P_0 and P_{20} samples.

Table 2 – Roughness results (R_a and R_t) of the top and lateral surfaces of P_0 and P_{20} samples.

Roughness (µm)		P_0		P_{20}	
		Top	Lateral	Top	Lateral
R_a	Average	12.47	11.83	10.52	9.46
	Standard deviation	0.77	1.87	0.48	0.96
R_t	Average	97.77	90.62	80.92	80.77
	Standard deviation	9.36	13.75	12.73	9.71

improve their geometrical quality (flatness and parallelism), as we analysed in a previous study [34]. Also, other parameters in which this improvement is reflected are roughness and porosity. Therefore, in this study, the influence of sandblasting on roughness and porosity was checked. The 25 mm size cubes were sandblasted evenly until an improvement of 20% on the top surface and 40% on the lateral surfaces of the samples was achieved for the R_a and R_t roughness parameters. This post-process reduced the total porosity of the samples by more than 35%. As a conclusion of this analysis, it has been found that the roughness and external porosity properties are closely linked and, of course, directly influenced by the application of the sandblasting post-processing, which gives the SLM parts a better surface finish on both parts (manufactured with P_0 and P_{20} powder).

3.3. *Microstructure and microhardness*

The microstructure of transversal (T_1) and longitudinal (L_1) sections after Vilella chemical etching is shown in Fig. 10. Transversal sections are characterised by footprints of visible laser tracks as parallel lines (Fig. 10a and Fig. 10c), while longitudinal sections are characterised by melting pools (Fig. 10b and Fig. 10d). The melting pools have a darker colour, surrounded by a lighter area on the edge.

The results of microhardness for both conditions (P_0 and P_{20}) were similar. The dark area exhibits an average microhardness value of 300 HV0.01 while. in the light area. The average value is 237 HV0.01. The microhardness values of the phases are independent of the type of powder and the analysed section (transversal or longitudinal).

The results of the XRD analysis for the P_0 and P_{20} samples are represented schematically in Fig. 11, both for lateral and top

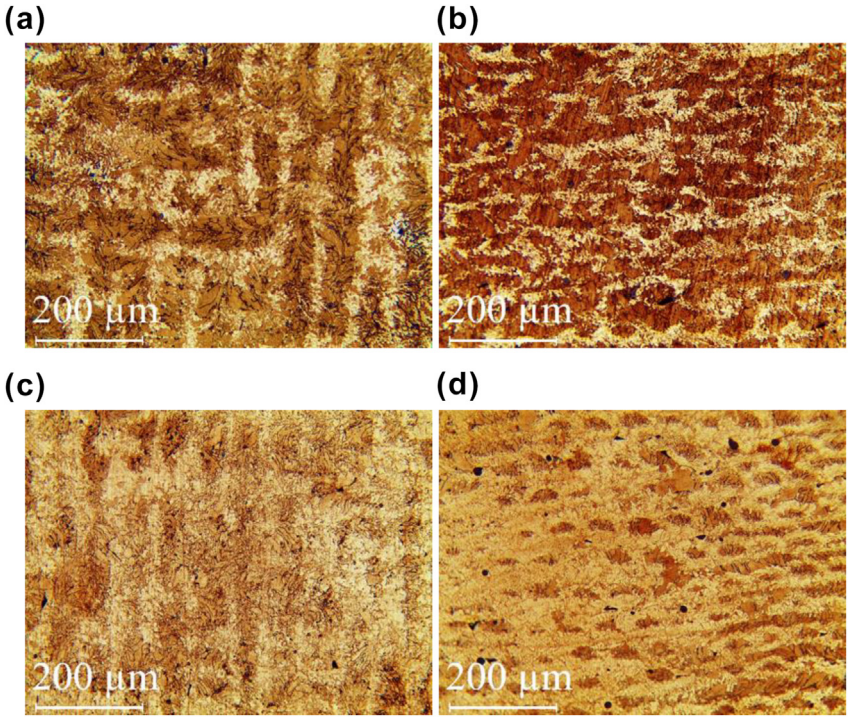

Fig. 10 – OM images with 100x magnification of surface microstructure. P_0 powder: (a) T_1 and (b) L_1; P_{20} powder: (c) T_1 and (d) L_1.

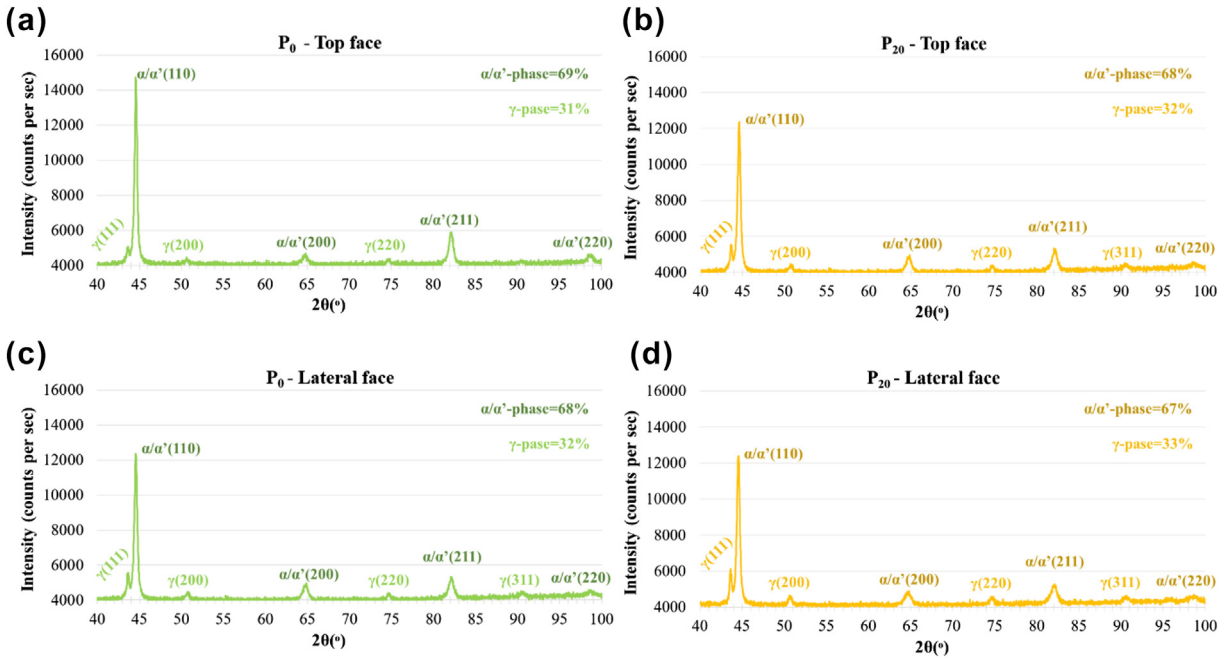

Fig. 11 – Schematic XRD results obtained on the top face of the samples: (a) P_0 and (b) P_{20}; and on the lateral face of the samples: (c) P_0 and (d) P_{20}.

Table 3 – Peak intensity ratios as a function of the analysed surface of the P_0 and P_{20} samples.

Surface		Peak intensity ratio (I/I_{max})							
		(111)	(110)	(200)	(200)	(220)	(211)	(311)	(220)
P_0	Top	35	**100**	30	31	30	40	–	32
	Lateral	45	**100**	36	40	35	43	36	37
P_{20}	Top	39	**100**	33	34	32	43	33	35
	Lateral	49	**100**	38	39	37	43	38	38

Table 4 – Hardness results of the T_1, T_2, L_1 and L_2 surfaces of P_0 and P_{20} samples.

Section	P0				P20			
	Transversal		Longitudinal		Transversal		Longitudinal	
	T_1	T_2	L_1	L_2	T_1	T_2	L_1	L_2
HV2	331	347	335	329	318	322	321	317
Average	339		332		320		319	

faces. The phase proportions are very similar for the two powder states (virgin and 20 times reused powder) and for the different faces (lateral and top surfaces). A slight increase in the γ-phase is observed with the powder reuse, obtaining an average value of 31.5% in the P_0 sample and 32.5% in the P_{20} sample. Likewise, XRD analyses of the powder at different recycling states also shows a slight increase in the proportion of the γ-phase [19]. This slight variation in phase proportions results in variations of mechanical properties, as discussed in the following sections.

XRD patterns (Fig. 11) show the presence of peaks related to both austenite (γ-phase) and martensite or ferrite (α-phase). Due to the very low carbon concentration (<0.04% by weight [19]) of the used 17-4 PH steel powder, the magnitude of lattice distortion in Body Centred Tetragonal (BCT) martensite was very small and it was not possible to distinguish between Body Centred Cubic (BCC) ferrite and BCT martensite [24].

Furthermore, the peak intensity ratios (I/I_{max}) of the 17-4 PH steel samples were calculated as a function of the analysed surface (top and lateral) (Table 3). No significant changes in the I/I_{max} ratio were observed, with respect to the type of powder used in manufacturing, as shown in Table 3. Regardless of the sample, the (110) plane has the maximum peak intensity ratio (I/I_{max}) between atomic planes (Fig. 11 and Table 3).

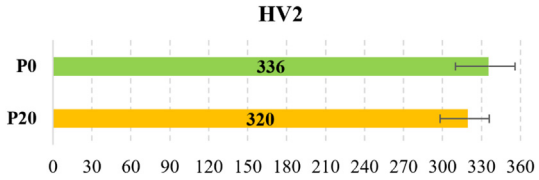

Fig. 12 – Hardness results on P_0 and P_{20} samples.

3.4. Hardness

The hardness of the different samples varies slightly, reaching average values of 336 and 320 HV2 in P_0 and P_{20} states, respectively (Fig. 12). As shown in Table 4, the mean values of nine measurements made on each sample are slightly higher for virgin powder samples. On the other hand, there is no relationship between the hardness and the analysed section on the part. Values of hardness obtained in the transversal (T_1

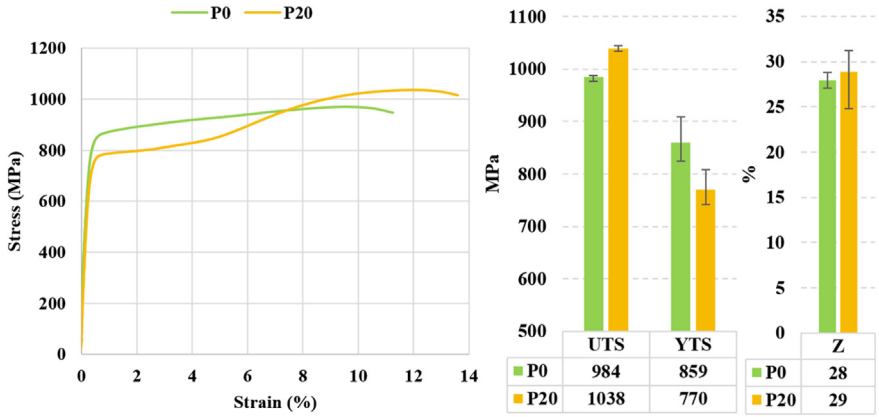

Fig. 13 – Tensile test results of P_0 and P_{20} samples (stress–strain curve, UTS, YTS and Z).

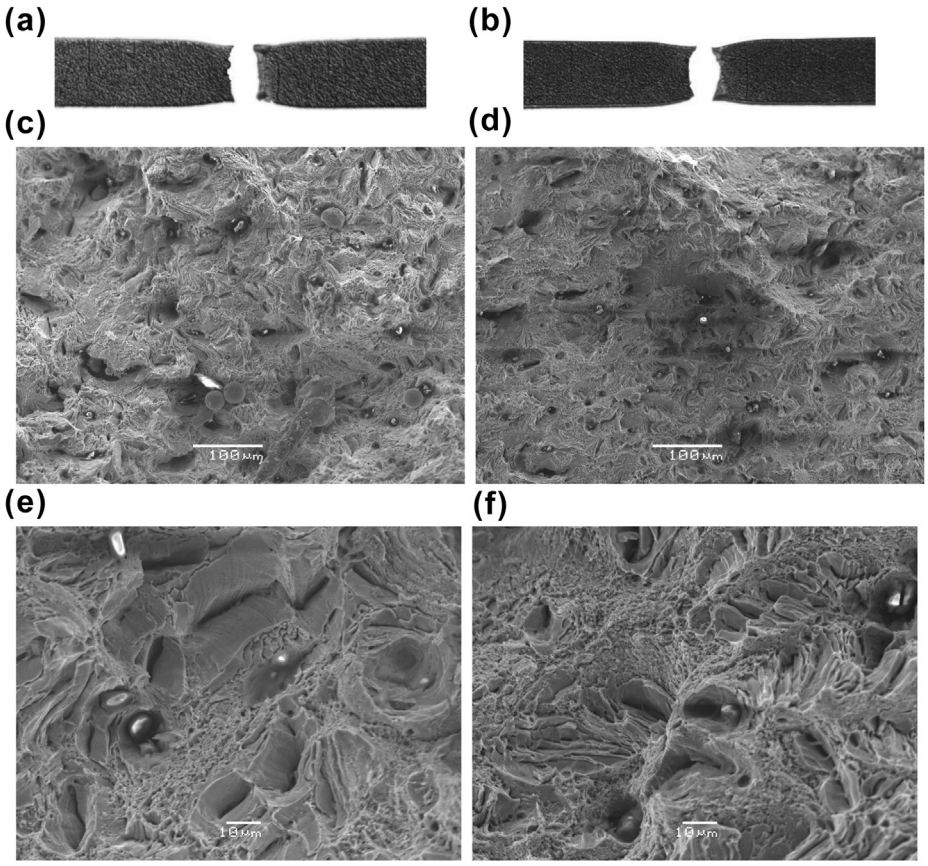

Fig. 14 – Tensile fracture surface: (a) P_0 and (b) P_{20} samples. SEM images of tensile fracture surfaces at 200x ((c) P_0 and (d) P_{20}) and 1000x ((e) P_0 and (f) P_{20}) magnifications.

and T_2) and longitudinal (L_1 and L_2) directions do not show significant differences (Table 4).

3.5. *Tensile strength*

Figure 13 shows the average values of tensile strength from the testing performed on the three samples manufactured with P_0 and P_{20} powder. The tensile behaviour changes with the powder state. The UTS is approximately 54 MPa higher in P_{20} than in P_0 samples, while YTS is about 89 MPa lower in P20 than P0. The percentage reduction of area (Z) value is similar in both parts (close to 30%).

These results agree with the hardness values obtained in the previous section (Fig. 12). Parts manufactured with reused powder are more ductile (therefore less hard) than in the case of virgin powder.

Figure 14a and Fig. 14b show the reduction of area produced in the tensile tests (P_0 and P_{20} states respectively). The SEM images of tensile fracture surfaces at different magnifications for P_0 (Fig. 14c and Fig. 14e) and P_{20} (Fig. 14d and Fig. 14f), show porosity due to LOF or gas trapped during the 3D printing process, as well as inclusions (unmelted powder and spatter particles), which cause the nucleation of voids until they coalesce. Regardless of the starting powder condition, there are no appreciable changes in either the morphology or voids size.

4. Conclusions

In order to analyse the influence of recycling the 17-4 PH stainless steel powder on the quality of the manufactured parts and continuing previous research on the characterisation of powder in different degrees of recycling, this paper focuses on the evaluation of SLM manufactured parts using 17-4 PH stainless steel powder in a virgin state (P_0) and 20 times reused (P_{20}).

A porosity analysis of the P_0 and P_{20} parts revealed a decrease in pore size (both the maximum and the average value) with powder reuse. In the case of virgin powder parts, the pore size is between 0.5 and 6535 μm^2 with an average value of 82 μm^2, while the pore size of P_{20} parts varies between 0.5 and 4542 μm^2 and an average value of 50 μm^2. With a decrease in pore size, both the number and circularity of pores increase. Therefore, the pores for the P_{20} parts have a slightly higher circularity (0.81) compared to the P_0 parts (0.78). The external or open porosity of the samples is practically the same in both powder states (about 0.80%); however, the internal or closed porosity varies from 0.39% (in virgin powder samples) to 0.24% (in reused powder samples). This difference is reflected in the total porosity of the SLM parts, which is reduced by 0.16% after 20 reuses of the raw material, varying the parts' density from 98.82% (P_0) to 98.98% (P_{20}).

The surface finish of SLM parts is characterised by high roughness, mainly due to the nature of the AM process (layer by layer), the SLM process parameters and the powder morphology. The average values of R_a and R_t were 12 μm and 92.57 μm, in the P_0 samples, and 9.75 μm and 80.81 μm, in the P_{20} samples, respectively. This shows that the more irregular morphology of the reused powder, compared to the virgin powder, slightly favours the improvement of the surface finish, as well as the decrease in the porosity of the manufactured parts. As expected, the highest roughness values were obtained on the top surface of the parts for both powder states, as it is the surface where the marks of the laser scanning strategy become visible.

Directly related to the surface quality of SLM parts, the influence of sandblasting post-processing on the roughness and open porosity properties of the parts (P_0 and P_{20}) was verified. This mechanical post-processing directly influenced both properties, resulting in a reduction of open porosity greater than 35% and, in the case of roughness, a reduction of 20% on the top surface and 40% on the lateral surfaces of the samples.

The microstructural analysis of both powder conditions (P_0 and P_{20}) does not present notable differences. A slight increase in γ-phase is observed with metallic powder reuse. XRD patterns show an approximate proportion of 68% α-phase (martensite or ferrite) and 32% γ-phase (austenite).

Regarding the mechanical properties, the reuse of metallic powder slightly influences both the tensile behaviour and the hardness. UTS increases with the powder reuse, reaching 984 MPa in P_0 parts and 1038 MPa in P_{20} parts. On the other hand, YTS decreases from 859 MPa to 770 MPa with powder reuse, keeping the area reduction percentage at a constant value close to 30%. These results show an increase in ductility of SLM parts with powder reuse and, therefore, a decrease in hardness, reaching a value of 336 HV2 in P_0 samples and 320 HV2 in P_{20} samples.

In conclusion, in SLM additive manufacturing processes, the reuse of 17-4 PH stainless steel powder is recommended to ensure an economic and environmental viability of the process. Both reused powder (even after 20 uses) and a mixture of reused and virgin powder can be used without significantly affecting the properties of the printed parts. The recycling process consists of recovering the unmolten powder by applying a vacuum, sieving it with a 75 μm mesh sieve, applying heat and loading it into the powder store of the SLM machine again.

In terms of future work, we propose the evaluation of the influence of both the SLM process parameters and the SLM post-processes (mechanical and heat treatments) on the properties of the printed parts, in order to optimise the entire manufacturing process.

Declaration of Competing Interest

The authors declare that they have no known competing financial interests or personal relationships that could have appeared to influence the work reported in this paper.

Acknowledgments

The authors gratefully acknowledge the financial support provided by the Junta de Castilla y León and FEDER (project ref. LE027P17).

REFERENCES

[1] Schiltz J, Alamos F, Kozlovsky K, Attardo R, Gatrell BA, Budzinski J, et al. Fatigue performance of direct metal laser sintered parts using reused metallic feedstocks. Procedia Manuf 2020;48:814–20. https://doi.org/10.1016/j.promfg.2020.05.118.

[2] Dowling L, Kennedy J, O'Shaughnessy S, Trimble D. A review of critical repeatability and reproducibility issues in powder bed fusion. Mater Des 2020;186:108346. https://doi.org/10.1016/j.matdes.2019.108346.

[3] Montelione A, Ghods S, Schur R, Wisdom C, Arola D, Ramulu M. Powder reuse in electron beam melting additive manufacturing of Ti6Al4V: particle microstructure, oxygen content and mechanical properties. Addit Manuf 2020;35:101216. https://doi.org/10.1016/j.addma.2020.101216.

[4] Sutton AT, Kriewall CS, Karnati S, Leu MC, Newkirk JW, Everhart W, et al. Evolution of AISI 304L stainless steel part properties due to powder recycling in laser powder-bed fusion. Addit Manuf 2020;36:101439. https://doi.org/10.1016/j.addma.2020.101439.

[5] Ghods S, Schur R, Schultz E, Pahuja R, Montelione A, Wisdom C, et al. Powder reuse and its contribution to porosity in additive manufacturing of Ti6Al4V. Materialia 2021;15:100992. https://doi.org/10.1016/j.mtla.2020.100992.

[6] Tang HP, Qian M, Liu N, Zhang XZ, Yang GY, Wang J. Effect of powder reuse times on additive manufacturing of Ti-6Al-4V by selective electron beam melting. J Occup Med 2015;67:555–63. https://doi.org/10.1007/s11837-015-1300-4.

[7] Sutton AT, Kriewall CS, Karnati S, Leu MC, Newkirk JW. Characterization of AISI 304L stainless steel powder recycled in the laser powder-bed fusion process. Addit Manuf 2020;32:100981. https://doi.org/10.1016/j.addma.2019.100981.

[8] Wang D, Ye G, Dou W, Zhang M, Yang Y, Mai S, et al. Influence of spatter particles contamination on densification behavior and tensile properties of CoCrW manufactured by selective laser melting. Opt Laser Technol 2020;121:105678. https://doi.org/10.1016/j.optlastec.2019.105678.

[9] Ahmed F, Ali U, Sarker D, Marzbanrad E, Choi K, Mahmoodkhani Y, et al. Study of powder recycling and its effect on printed parts during laser powder-bed fusion of 17-4 PH stainless steel. J Mater Process Technol 2020;278:116522. https://doi.org/10.1016/j.jmatprotec.2019.116522.

[10] Gorji NE, O'Connor R, Mussatto A, Snelgrove M, González PGM, Brabazon D. Recyclability of stainless steel (316 L) powder within the additive manufacturing process. Materialia 2019;8:100489. https://doi.org/10.1016/j.mtla.2019.100489.

[11] Terrassa KL, Haley JC, MacDonald BE, Schoenung JM. Reuse of powder feedstock for directed energy deposition. Powder Technol 2018;338:819–29. https://doi.org/10.1016/j.powtec.2018.07.065.

[12] Heiden MJ, Deibler LA, Rodelas JM, Koepke JR, Tung DJ, Saiz DJ, et al. Evolution of 316L stainless steel feedstock due to laser powder bed fusion process. Addit Manuf 2019;25:84–103. https://doi.org/10.1016/j.addma.2018.10.019.

[13] Yi F, Zhou Q, Wang C, Yan Z, Liu B. Effect of powder reuse on powder characteristics and properties of Inconel 718 parts produced by selective laser melting. J Mater Res Technol 2021;13:524–33. https://doi.org/10.1016/j.jmrt.2021.04.091.

[14] Alamos FJ, Schiltz J, Kozlovsky K, Attardo R, Tomonto C, Pelletiers T, et al. Effect of powder reuse on mechanical properties of Ti-6Al-4V produced through selective laser melting. Int J Refract Met Hard Mater 2020;91:105273. https://doi.org/10.1016/j.ijrmhm.2020.105273.

[15] Pinto FC, Souza Filho IR, Sandim MJR, Sandim HRZ. Defects in parts manufactured by selective laser melting caused by δ-ferrite in reused 316L steel powder feedstock. Addit Manuf 2020;31:100979. https://doi.org/10.1016/j.addma.2019.100979.

[16] Ardila LC, Garciandia F, González-Díaz JB, Álvarez P, Echeverria A, Petite MM, et al. Effect of IN718 recycled powder reuse on properties of parts manufactured by means of Selective Laser Melting. Phys Procedia 2014;56:99–107. https://doi.org/10.1016/j.phpro.2014.08.152.

[17] Cordova L, Bor T, de Smit M, Carmignato S, Campos M, Tinga T. Effects of powder reuse on the microstructure and mechanical behaviour of Al–Mg–Sc–Zr alloy processed by laser powder bed fusion (LPBF). Addit Manuf 2020;36:101625. https://doi.org/10.1016/j.addma.2020.101625.

[18] Powell D, Rennie AEW, Geekie L, Burns N. Understanding powder degradation in metal additive manufacturing to allow the upcycling of recycled powders. J Clean Prod 2020;268:122077. https://doi.org/10.1016/j.jclepro.2020.122077.

[19] Zapico P, Giganto S, Barreiro J, Martínez-Pellitero S. Characterisation of 17-4PH metallic powder recycling to optimise the performance of the selective laser melting process. J Mater Res Technol 2020;9:1273–85. https://doi.org/10.1016/j.jmrt.2019.11.054.

[20] 3D Systems. Direct metal printers. Metal additive manufacturing with the ProX DMP 3D printers. 2017.

[21] Zapico P, Giganto S, Martínez-Pellitero S, Fernández-Abia AI, Castro-Sastre MÁ. Influence of laser energy in the surface quality of parts manufactured by selective laser melting. Ann DAAAM Proc Int DAAAM Symp 2018:279–86. https://doi.org/10.2507/29th.daaam.proceedings.040.

[22] Rashid R, Masood SH, Ruan D, Palanisamy S, Rahman Rashid RA, Elambasseril J, et al. Effect of energy per layer on the anisotropy of selective laser melted AlSi12 aluminium alloy. Addit Manuf 2018;22:426–39. https://doi.org/10.1016/j.addma.2018.05.040.

[23] Kudzal A, McWilliams B, Hofmeister C, Kellogg F, Yu J, Taggart-Scarff J, et al. Effect of scan pattern on the microstructure and mechanical properties of Powder Bed Fusion additive manufactured 17-4 stainless steel. Mater Des 2017;133:205–15. https://doi.org/10.1016/j.matdes.2017.07.047.

[24] Sun Y, Hebert RJ, Aindow M. Effect of heat treatments on microstructural evolution of additively manufactured and wrought 17-4PH stainless steel. Mater Des 2018;156:429–40. https://doi.org/10.1016/j.matdes.2018.07.015.

[25] Jandaghi MR, Saboori A, Iuliano L, Pavese M. On the effect of rapid annealing on the microstructure and mechanical behavior of additively manufactured stainless steel by Laser Powder Bed Fusion. Mater Sci Eng, A 2021;828:142109. https://doi.org/10.1016/j.msea.2021.142109.

[26] 3D Systems. LaserForm ® 17-4PH (B) for ProX® DMP 100, 200 and 300 direct metal printers general. 2017.

[27] Pasebani S, Ghayoor M, Badwe S, Irrinki H, Atre SV. Effects of atomizing media and post processing on mechanical properties of 17-4 PH stainless steel manufactured via selective laser melting. Addit Manuf 2018;22:127–37. https://doi.org/10.1016/j.addma.2018.05.011.

[28] Dehghan-Manshadi A, Yu P, Dargusch M, StJohn D, Qian M. Metal injection moulding of surgical tools, biomaterials and medical devices: a review. Powder Technol 2020;364:189–204. https://doi.org/10.1016/j.powtec.2020.01.073.

[29] de Terris T, Andreau O, Peyre P, Adamski F, Koutiri I, Gorny C, et al. Optimization and comparison of porosity rate measurement methods of Selective Laser Melted metallic parts. Addit Manuf 2019;28:802–13. https://doi.org/10.1016/j.addma.2019.05.035.

[30] ISO 4288. Geometrical Product Specifications (GPS) — surface texture: profile method — rules and procedures for the assessment of surface texture 1996. 1996.
[31] ASTM E975-13. Standard practice for X-ray determination of retained austenite in steel with near random crystallographic orientation. 2013.
[32] ISO 6892-1:2019. Metallic materials – tensile testing – Part 1: method of test at room temperature 2019.
[33] Zhang B, Li Y, Bai Q. defect formation mechanisms in selective laser melting: a review. Chinese J Mech Eng (English Ed 2017;30:515–27. https://doi.org/10.1007/s10033-017-0121-5.
[34] Cuesta E, Alvarez BJ, Zapico P, Giganto S. Analysis of post-processing influence on the geometrical and dimensional accuracy of selective laser melting parts. Rapid Prototyp J 2020;26:1713–22. https://doi.org/10.1108/RPJ-02-2020-0042.